Chapter 2

Surface engineered porous magnetic graphitic sheets for rapid and efficient recovery of oil

As the demand for fossil fuels is ever increasing and supply as form of oil reserves are decreasing with time, there is an urgent need for increase in efficiency of sorbent material production. Low capture performance and low specific surface area with less micro-pore proportion of the available absorbent materials are the key drawbacks that hamper their practical applications in crude oil removal. To overcome the aforementioned challenges and in order to improve the oil sorption performances, two dimensional (2D) layered materials, due to their specific surface area, are considered as novel and suitable candidate towards sorption processes. This chapter discusses development of magnetic hydrophobic/oleophilic g-C_3N_4 nanocomposite that exhibit excellent oil sorption performance and rapid removal of adsorbed oil using an external magnet. Combining porous and nanosheets structure along with magnetic $FeNi_3$ and fatty acid surface functionalization make the system an efficient adsorbent for adsorbing and separating crude oil from water. The developed nanocomposite can be further recycled and reused for significant recovery of oil. Moreover, the chapter is divided into two parts: Part A and Part B. Part A consist of experimental and Part B theoretical analysis.

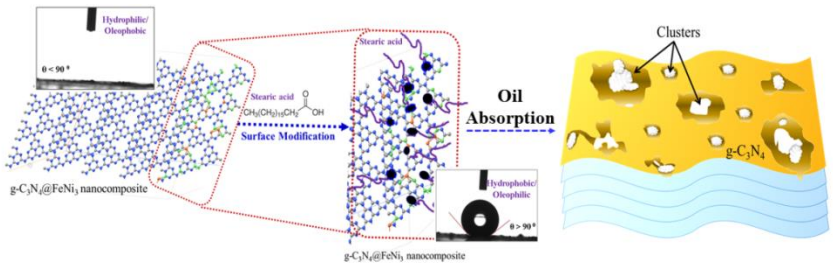

Figure 2.1: Schematic description of oil-water separation by g-C_3N_4@$FeNi_3$ nanocomposite.

This portion of the thesis is published in M. Talukdar et al. *Applied Surface Science* **473** (2019) 275–281

2.1 Introduction

Recovery of crude oil and separation from oil-water mixture is one of the most promising fields of research in industrial and environmental chemistry [1-3]. In oil drilling, transportation and refining processes, a huge amount of oil is wasted as oil is mixed with mud, sand, water and some other unwanted agents. As the demands for fossil fuels are ever increasing and the supply as form of oil reserves are decreasing with time, there is a need for increase in production. The supply of oil can be greatly increased in this hour of need by employing efficient recovery techniques. This is a very important task as the wastage of oil is linked to some major environmental pollution issues such as soil and marine water pollution. Because of marine water pollution, birds, mammals such as whale, fishes and a large number of aquatic animals lose their life every year. The cause of toxicity is far reaching as the moving water carries the contamination to a large area causing adverse effect on its biodiversity. This requires prompt oil recovery and removal of contaminated oil in a very efficient way. Traditionally, many methods are followed in case of oil water separations. Though one way to clean-up oil spilled water is using a series of hydrophobic and oleophilic absorbents, including activated carbon, zeolites, natural fibers, magnetic particles but all these undergo low separation and absorption efficiency. Numbers of materials have been developed to overcome these principal drawbacks, but the outcome in terms of materials cycling ability is unsatisfactory [4-6]. However, due to high viscosity of crude oil, these advanced absorbent materials hinder the practical application. Indeed, besides good absorbing properties in terms of capacity and kinetics, the desired absorbent materials should exhibit light weight for high gravimetric capacity, easy separation from cleaned water and easy cleaning for long-term cycling. In order to deal with the pertinent environmental pollution, search for hunting smart materials for efficient separation and removal of oil from water are highly essential. Many materials including clay minerals and nonwoven fabrics have been used to absorb oily compounds from water [7-9]. However, during separation, the material absorbs both oil and water which decreases their efficiency and selectivity. In this regard, few of the synthetic and

natural sorption materials with both hydrophobic and oleophilic properties have been investigated and tested for oil-removal purpose [10-14]. An active area of research in this aspect is to optimize adsorption performance, where the surface area plays major role [15]. Primarily, they should be developed with high specific surface area and large proportion of meso-pores. As a noteworthy, layered two dimensional (2D) materials has attracted much attention recently owing to their excellent physical properties such as high carrier mobility, photoconductivity, environmental sensitivity, and mechanical properties. They have been marked as great potential towards adsorption processes due to its high surface to volume ratio, unlike its bulk form [16-17]. Besides, high content of carbon and nitrogen are preferred to be present as a prerequisite in the adsorbent moiety which highly boosts its efficacy.

In this chapter, we have developed the strategy (as shown in **Figure 2.1**) of employing graphitic C_3N_4, which provides high surface area owing to its 2D sheet structure. In the present study, nontoxic iron nickel ($FeNi_3$) magnetic nanoparticles (MNPs) have been mixed with graphitic carbon nitride (g-C_3N_4) to form the composite material. The layers in g-C_3N_4 sheet are connected via tertiary amines in a stacked fashion and separated by weak van der Waals (vdW) forces. Moreover, $FeNi_3$ MNPs are uniform delocalization (i.e., the distribution of magnetic spheres) over the sheet surface, enhancing the sorption capability of the host flakes. Besides, the nanocomposite exhibits hydrophobic and oleophilic properties after surface engineering with stearic acid ($CH_3(CH_2)_{16}COOH$), which makes the oil extraction easy and effective. Moreover, the nanocomposite efficiently removes variety of oils from water surface under an external magnet.

Part A

2.2 Chemicals and materials used

Precursors like, Sodium Acetate ($C_2H_3NaO_2$), Ethylene glycol ($C_2H_6O_2$)), Ferric chloride ($FeCl_3$), Nickel chloride hexahydrate ($NiCl_26H_2O$), Urea (CH_4N_2O), Ethanol (C_2H_6O), Diphenyl ether ($C_{12}H_{10}O$), Hydrazine (N_2H_4) chemicals with 99.97% purity from Merck were used during synthesis. Stearic acid

($CH_3(CH_2)_{16}COOH$) from Loba Chemie has been used for surface modification of g-C_3N_4 sheet. Double distilled water was used for washing purposes during the synthesis process. The experiments were repeated for three times to achieve the uncertainties in the results.

2.2.1 Preparation of $FeNi_3$

$FeNi_3$ nanoparticles were synthesized by hydrothermal method. $FeCl_3$ and $NiCl_26H_20$ were mixed in 80 ml of ethylene glycol at room temperature in this synthesis method. Hydrazine was added to the solution after one hour of vigorous stirring and kept the solution stand still for another one hour. Then, the solution was moved to an autoclave and placed in the oven for 10 hours at 180^0C. The collected solution was centrifuged to obtain the precipitate. The precipitate was further washed with ethanol and the obtained black colored final precipitate was dried at 60^0C.

2.2.2 Preparation of graphitic carbon nitride (g-C_3N_4) sheet

2D graphitic carbon nitride was prepared by pyrolysing urea. The g-C_3N_4 sheet like structure was obtained by calcination of urea at 500^0C. After 4 hours of heating, the sample was allowed to cool down to room temperature and collected. The collected sample was centrifuged to obtain the precipitate. The precipitate was further washed with double distilled water and the obtained precipitate was dried at a mild temperature of 60^0C to obtain the final product of g-C_3N_4 sheet.

2.2.3 Preparation of composite g-C_3N_4@$FeNi_3$

The composite of $FeNi_3$ and graphitic carbon nitride were synthesized by physical blending method. Both g-C_3N_4 and $FeNi_3$ are taken with 1:1 molar ratio for composite formation.

2.2.4 Surface modification of the prepared nanocomposite

For making the composite oleophilic in nature, the sheet surface was modified with fatty acid named stearic acid. A mixture of nanocomposite to stearic acid with 1:8 molar ratio was taken with ethanol and placed in a shaker for proper mixing. The mixture was centrifuged to collect the precipitate and further washed with ethanol. The collected precipitate was then dried at a temperature of 60^0C.

2.2.5 Crude oil

The crude oil has been collected from Duliajan Oil Refinery, which is located in Dibrugarh District of Assam state in India. The oil that was collected was highly viscous in nature. It contained crude oil mixed with mud which was extracted from underground. The viscosity of crude oil was reduced by mixing an appropriate amount of diphenyl ether. The mixture was sonicated for 15 minutes before performing the experiments.

2. 3 Results and Discussion

2.3.1 Microstructure and Surface morphology

Micro-structural study of the composite was carried out through x-ray diffraction as shown in **Figure 2.2.** In case of $FeNi_3$ magnetic nanoparticles, the peaks at 2θ=44.10, 51.30 and 75.70 were indexed to (111), (200) and (220) lattice plane reflections respectively (**Figure 2.2 a**) indicating face-centered cubic structure (JCPDS card No. 38-0419). The diffraction peaks observed for graphitic carbon nitride sheet (**Figure 2.2 b**) at 2θ value 12.80 and 27.40 corresponds to the lattice plane (100) and (002) respectively (JCPDS card No. 87-1526). All peaks were assigned to the existence of $FeNi_3$ and g-C_3N_4 phases in the composite system (**Figure 2.2 c**). In case of composite system, diffraction peaks observed at 2θ= 12^0, 27.4^0, 44.1^0, 51.3^0 and 75.7^0 indexed to (100), (002), (111), (200) and (220) lattice planes, respectively. The above results endorsed the formation of g-C_3N_4@$FeNi_3$ composite. However, the peak intensity became weaker and the width of the

diffraction peak became broader indicating interactions between magnetic nanoparticles and host sheet due to presence of Fe and Ni in the composite system. Also, the characteristic peak intensity of (002) plane gets relatively suppressed, which further reveals the formation of the nanocomposite.

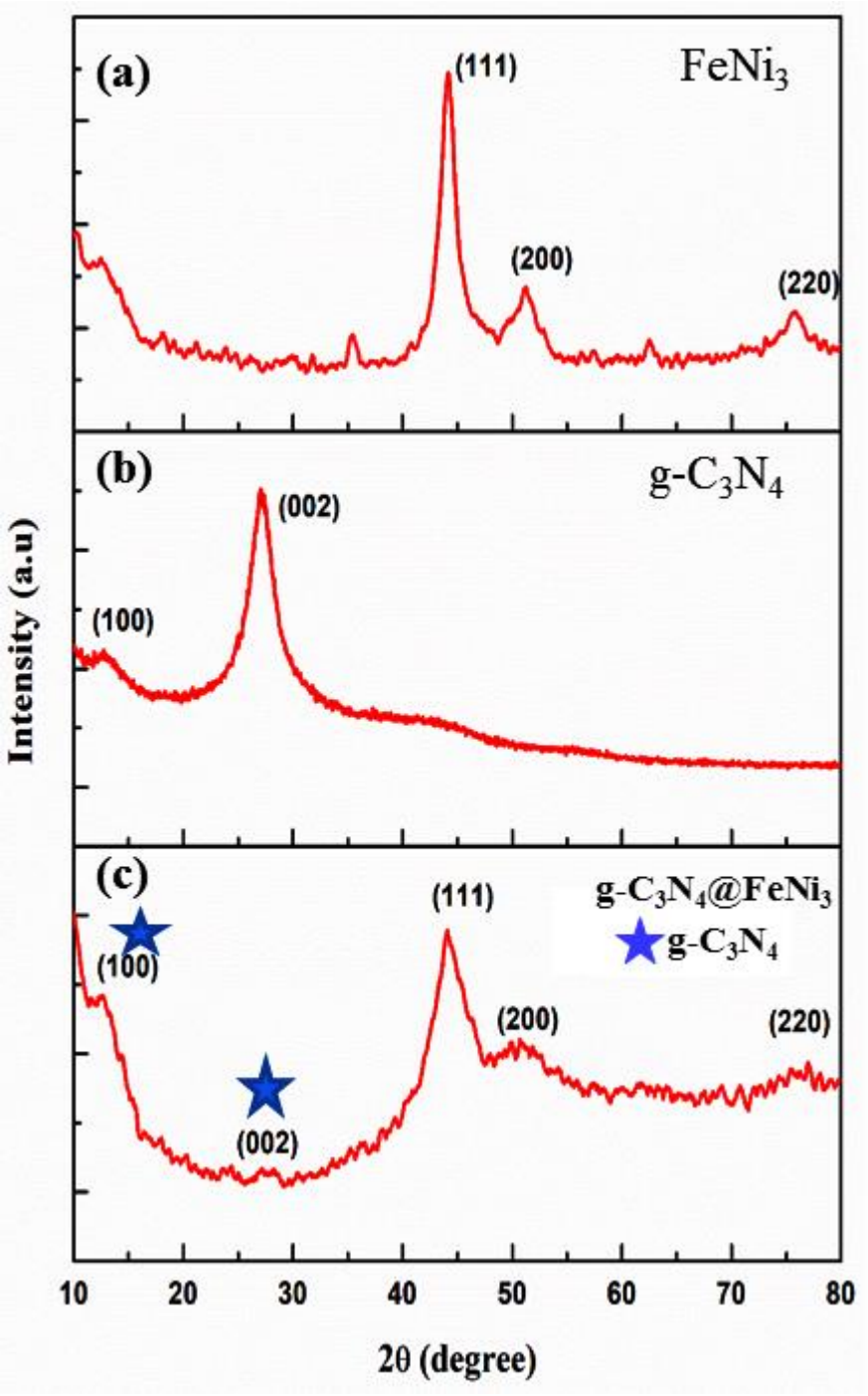

Figure 2.2: XRD plots of **(a)** $FeNi_3$ **(b)** g-C_3N_4 and **(c)** g-C_3N_4@$FeNi_3$ nanocomposite.

A representative TEM image of the composite system before surface modification was shown in **Figure 2.3 (a)** with its SAED pattern **Figure 2.3 (b)**. The image revealed uniformity in shape and size of MNPs, with average diameter 70 nm over the sheet surface in the composite system. A stacked graphitic structure was noticed with the dispersion of MNPs on the carbon nitride sheets impeding the formation of composite system. SAED pattern indicated that the nanoparticles are polycrystalline in nature with respective planes of both $FeNi_3$ and g-C_3N_4 identified in the composite.

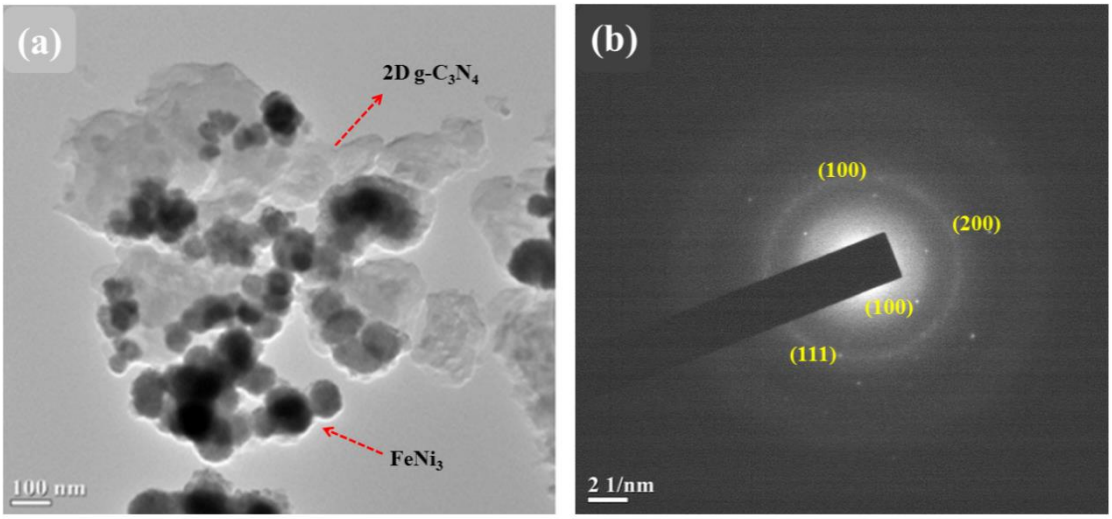

Figure 2.3: **(a)**TEM micrograph and **(b)** SAED pattern of g-C_3N_4@$FeNi_3$ nanocomposite before oil adsorbtion

AFM images of the system were shown in **Figure 2.4** to visualize the surface topography before (**Figure 2.4 (a and b)**) and after oil removal (**Figure 2.4 (c and d)**). AFM images provided convincing evidence regarding post-oil adsorption (**Figure 2.4 c**) enhancement in MNP size indicating the formation of finite number of nanoparticle clusters over the sheet surface. Also, the images revealed the uniform increase of nine times in thickness of the nanosheets after oil adsorption (**Figure 2.4 (d)**) compared to the pristine nanosheets (**Figure 2.4 (b)**). **Figure 2.4 (b) and (d)** identifies the surface topology of the system, where it identifies rough surface of adsorbent before oil adsorption. Also, the roughness decreases after oil adsorption.

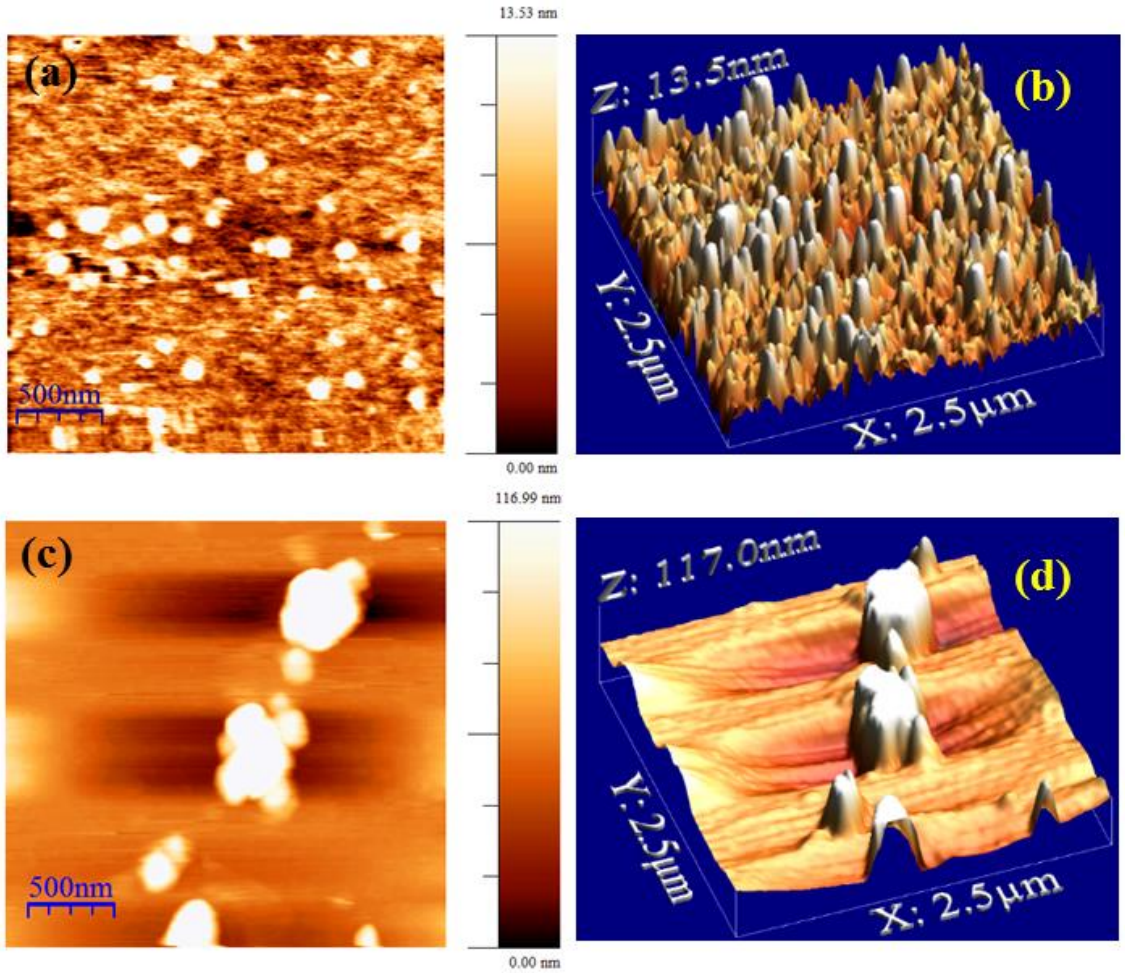

Figure 2.4: AFM images of the surface modified nanocomposite **(a)** phase profile **(b)** topology profile of before oil adsortion and **(c)** phase profile **(d)** topology profile of after oil adsorption embeded with their respective 3D image on the left top.

2.3.2 Porosity and surface area analysis

Figure 2.5 (a) displayed the adsorption-desorption isotherm curves of g-C_3N_4 sheet showing the characteristic of type IV isotherm pattern. The surface area was found to be 41 m^2 g^{-1} for g-C_3N_4 from the Brunauer-Emmett-Teller (BET) curve. Barrett-Joyner-Halenda (BJH) curve indicated the pore-size distribution of the flake reflecting the existence of mesopore in the flake structure (shown in **Figure 2.5 (b)**). The pore-size distribution curve showed the mesoporous structure with the pore size in the range of 4-40 nm. The textural property of the g-C_3N_4 @$FeNi_3$ is basically consistent with that of g-C_3N_4 support, suggesting that the $FeNi_3$ nanoparticles do not block the pore distribution on the sheet surface. Moreover,

the nitrogen adsorption-desorption curve shows smooth desorption-adsorption characteristics, which confirms that the prepared surface is free from significant defects.

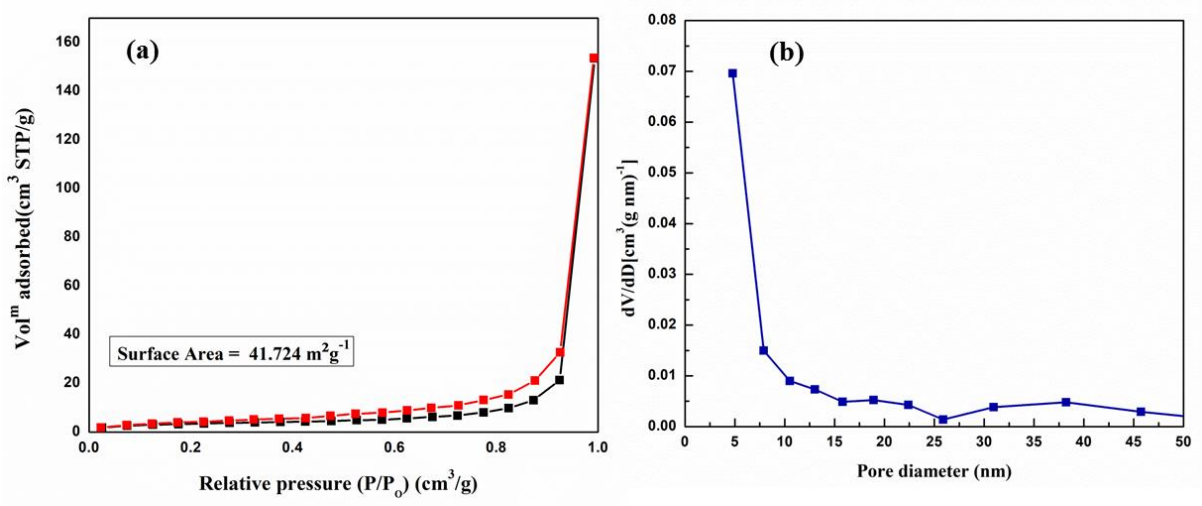

Figure 2.5: (a) BET adsorption–desorption isotherm and **(b)** BJH pore-size distribution analysis

2.3.3 Contact Angle analysis

Surface engineering enabled in wettability transition of the nanocomposite and was ensured by contact angle measurements before and after oil adsorption (shown in **Figure 2.6 (a) and (b)** respectively). Increase in contact angle upto 140^0 implied hydrophobic and oleophilic nature of the prepared nanocomposite material. Shape of water droplet above the sample was uniform, indicating surface to be highly hydrophobic. The composite retained its hydrophobic behaviour even after reusing for oil removal for a number of times. The nanocomposite maintained its hydrophobic and oleophilic behaviour after its first use which showed the surface transition in wettability nature due to good stearic acid-based surface engineering of the nanocomposite. Highly hydrophobic and oleophilic nanocomposite exhibited a selective absorbance for oil recovery. When brought into contact with layer of crude oil in oil-water mixture, the nanocomposite adsorbed the oil instantaneously repelling the water. Interestingly, the oil-adsorbed nanocomposite could be removed from oil-water mixture with an external magnet within a quick response. The process of oil adsorption and removal is shown in **Figure 2.6 c((i)-(iv))** in stepwise manner. The outcome

efficacy is realized through several major parameters such as enhancement in mass and thickness of the adsorbate after adsorption process and also the response time of magnetic separation. The surface engineered nanocomposite system showed oil adsorption capacity up to 4.5 times and 9 folds of its pristine system weight and thickness, respectively confirming the importance of the highly hydrophobic and oleophilic surfactant for selective oil adsorption. Apart from crude oil separation, other oils such as Mobil, petrol and mustard oil were also used in extraction process. It has been found that surface modified 2D g-C_3N_4@$FeNi_3$ can also be used to separate these varieties of oils.

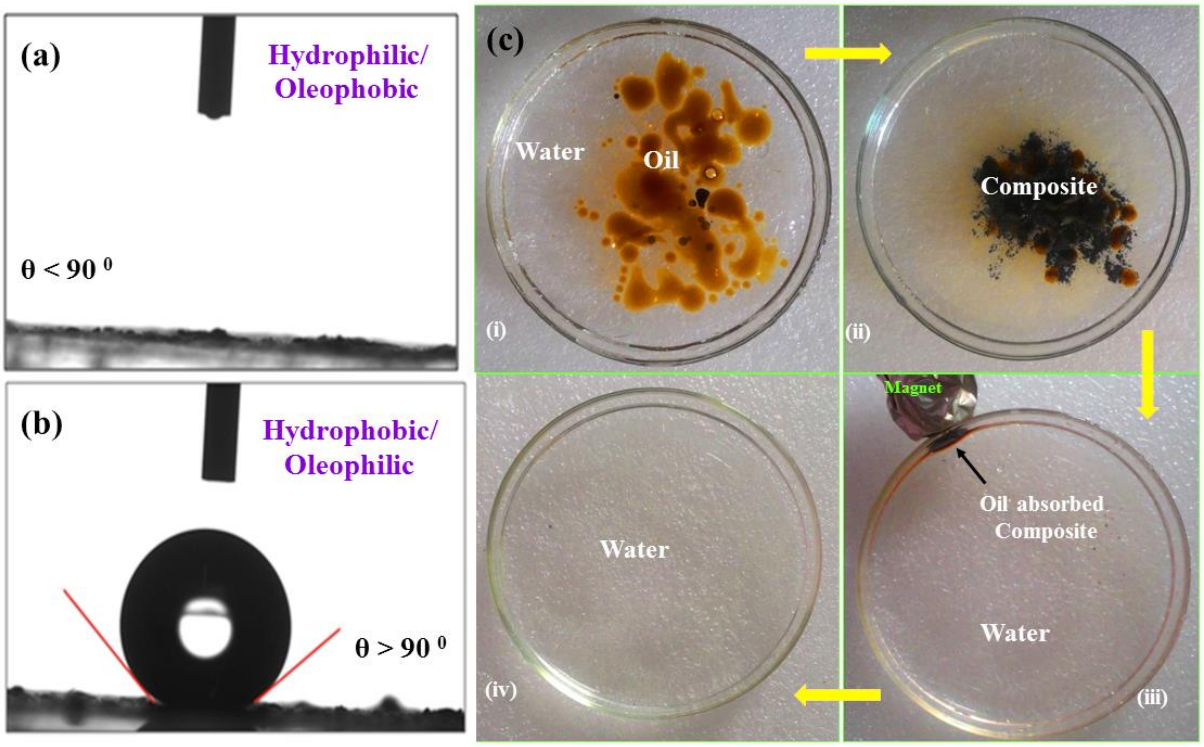

Figure 2.6: (a) hydrophilic/oleophobic surface of nanocomposite showing contact angle below 90^0 and **(b)** surface modified to hydrophobic/oleophilic showing contact angle above 90^0. **(c)** Removal process of crude oil ((i)-(iv)) from water surface by nanocomposite under magnetic field.

2.3.4 GC-MS analysis

The GC-MS characterization (**Figure 2.7**) was performed to confirm the adsorption of the viscous oil and its removal efficacy. It was observed that several chromatographic peaks were present revealing the existence of crude oil in the oil-water mixture before oil removal. The water, left-over in the Petri dish after oil adsorption, was tested again and found no such peaks. The absence of aforementioned peaks indicated the absence of oil in the oil water mixture showing efficient oil removal by the composite.

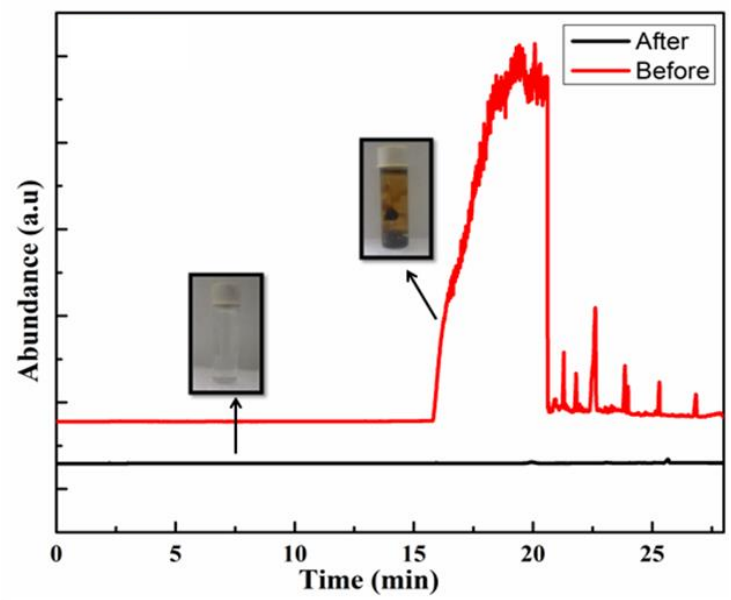

Figure 2.7: GC-MS plot of the surface modified composite before and after oil adsorptions.

2.4 Adsorption Kinetics

The adsorption kinetics is one of the important characteristics in defining and understanding adsorption mechanism [18-19]. So, the detailed adsorption kinetic study of oil adsorption using surface modified g-C_3N_4@$FeNi_3$ nanocomposite was performed. Pseudo first order and pseudo-second order kinetics has been carried out from the data obtained from experimental results to analyse the adsorption kinetics of the oil.

$$\log(m_2 - m_1) = \log m_2 - \frac{k_1}{2.303} t \ldots\ldots\ldots\ldots\ldots\ldots\ldots\ldots\ldots\ldots (1)$$

Equation (1) implies the pseudo first-order kinetic study where, m_1 and m_2 are the amounts (in gram) of before and after oil removal adsorbate at t sec, respectively. Here, k_1 is the rate constant of pseudo first- order adsorption. The calculated value of k_1 is 0.25.

Similarly, the pseudo second-order kinetics is shown in equation (2) below,

$$\frac{1}{m_1} = \frac{1}{m_2^2\, k_2} + \frac{1}{m_2} \ldots\ldots\ldots\ldots\ldots\ldots\ldots\ldots\ldots\ldots (2)$$

where, k_2 is the second order rate constant of adsorption. The calculated k_2 value is found to be 1.28, which is approximately 5 times larger than k_1 value (i.e., $k_2 > 5k_1$), corroborating the 4.5 times mass enhancement after oil adsorption by the nanocomposite. This result indicates that the oil adsorption by surface modified g-C_3N_4@$FeNi_3$ composite follows pseudo second-order kinetics rather than pseudo first-order kinetics [**Appendix A.1**]. Higher k_2 value from second order kinetic analysis is specifying the uniformity of binding energy over the entire adsorbate surface and there is no significant interaction between the adsorbate and water molecules indicating rapid removal of oil by the adsorbent (**Figure 2.8 (a) and (b)**). Moreover, the oil separation efficiency (92%, 94.2% and 100%) has been achieved with varying the weight percentage (0.09, 0.1 and 0.3 wt. %) of the composite system to separate oil (shown in **Figure 2.8(c and d)**), respectively.

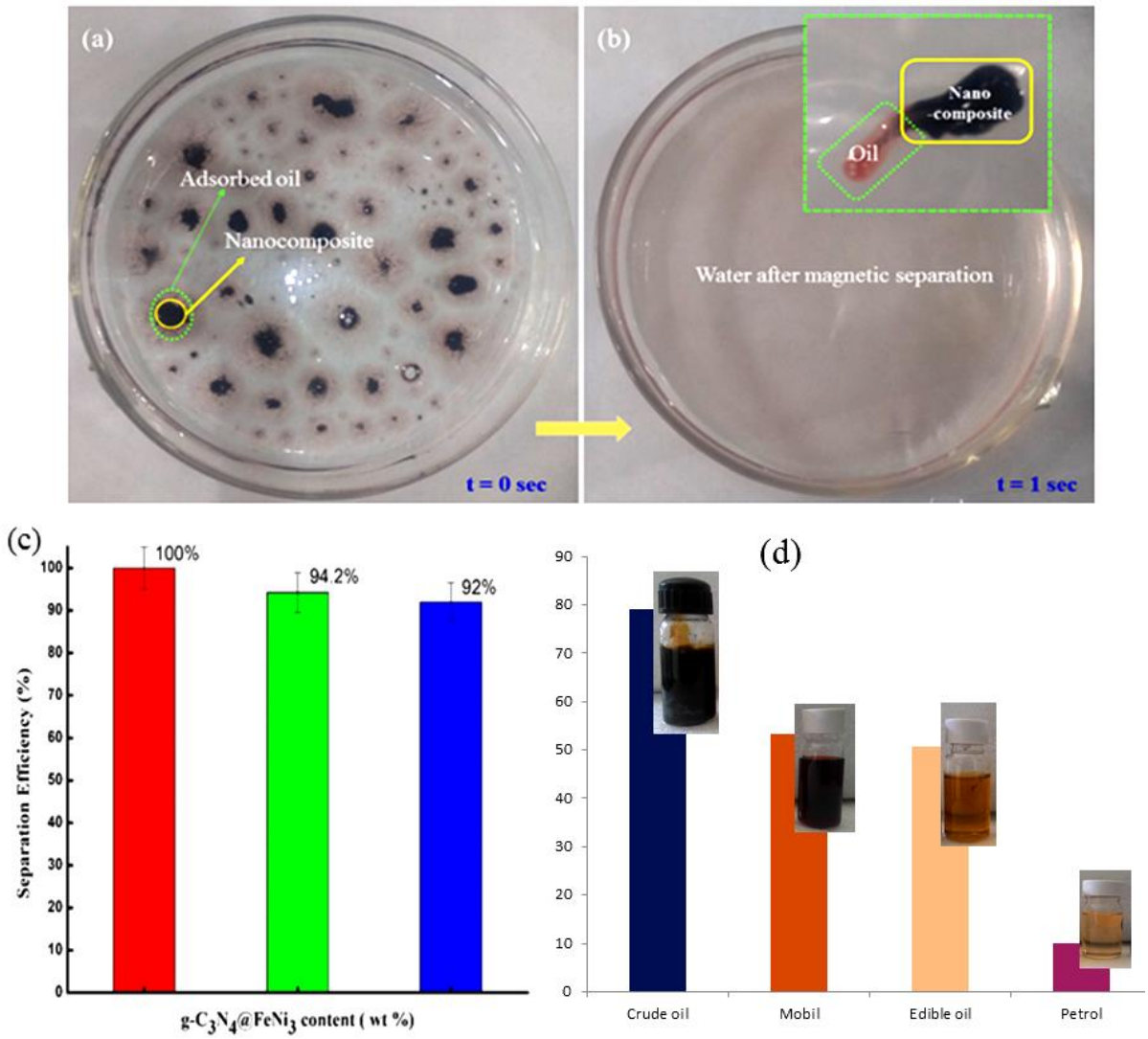

Figure 2.8: The surface adsorbed oil by nanocomposite **(a)** and the water after magnetic separation **(b)** with an inset showing the oil adsorbed nanocomposite (marked by dotted lines). The rapid response time for magnetic separation is shown in both the cases as t=0 sec and t=1 sec. **(c)** The separation efficiency as a function of wt. % of the g-C_3N_4@$FeNi_3$ composite system and **(d)** Adsorption of various forms of oil.

2.5 Adsorption Isotherm

Interaction between adsorbent and adsorbate can be realised by the adsorption isotherm at equilibrium of the adsorption process. Adsorption capacity of g-

C_3N_4@$FeNi_3$ system is calculated for all the three adsorption isotherms. The value of the correlation coefficient (R^2) for Freundlich equation for adsorption of oil is much higher than that for Langmuir and Temkin equation. The linearized mathematical expression of the Freundlich equation (3) is given below as,

$$log m_1 = \frac{1}{n} log(D_{equ.}) + log(K) \quad \ldots\ldots (3)$$

where, m_1 is the amount of adsorbate, $D_{equ.}$ (g/ml) is the equilibrium solute concentration in solution, and K and n are Freundlich constants related to adsorption capacity and adsorption intensity, respectively. Correlation coefficient of the oil adsorption process fits well with the Freundlich isotherm, indicating multilayer adsorption over engineered porous g-C_3N_4 surfaces with respect to the heat of adsorption.

2.6 Oil recovery and Reusability

The graphitic magnetic nanocomposite can be further recycled **Figure 2.9 (a)** and reused for oil adsorption and separation in an eco-friendly manner. The system can be further reused easily by washing the composite with ethanol and then drying at a temperature of 60^0C for few hours. Apart from the reusability of the nanocomposite, the removed oil can be recovered successfully. **Figure 2.9 (b and c)** shows the recovery of oil after separation.

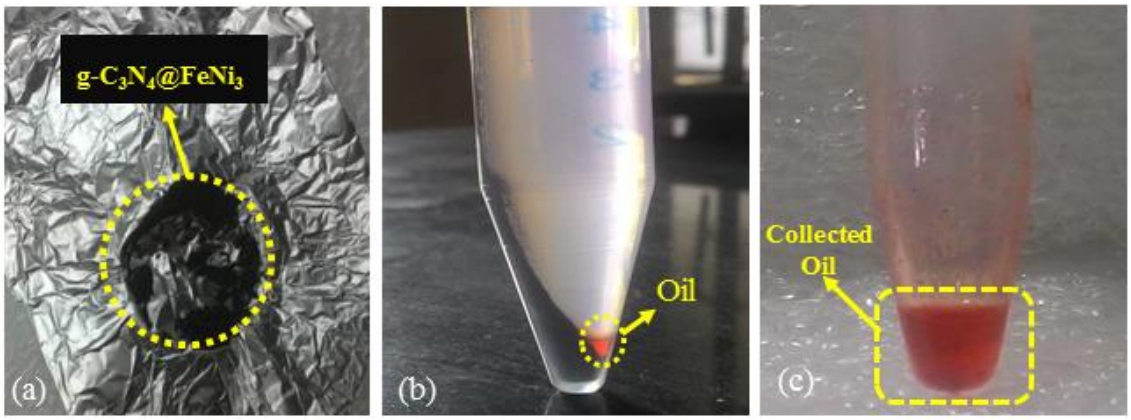

Figure 2.9: The collected surface modified g-C_3N_4@$FeNi_3$ nanocomposite **(a)** is washed **(b)** and oil is collected **(c)**.

Part B

2.7 Computational Details.

We carried out the electronic structure of the system using density functional theory calculation after obtaining fully relaxed crystal structure using the Quantum Espresso codes within generalized gradient approximation (GGA) following Perdew–Burke–Ernzerhof (PBE) format. The vdW-DF scheme was included for the van der Waals interaction. Lattice optimization was performed with a Monkhorst mesh of 9×9×1 k-points at 540 eV as plane wave cutoff energy. Hellmann-Feynman force was optimized to less than 0.001 eV/Å to get stable optimized geometry. A vacuum region of 12 Å in the z-direction was maintained to avoid periodic interaction between layers. We used 27 × 27 × 1 k-mesh and the triangular integration method to generate an accurate electronic density of states [20].

2.7.1 Atomic configuration of the system

The minimum energy-based structures of the composite system are fixed using geometry optimization via Broyden-Fletcher-Goldfarb-Shanno (BFGS) algorithm [21-22]. The geometry optimization is fixed via affecting the organizing atoms in the supercell to minimum total energy position for stable geometry (shown in **Figure 2.10**).

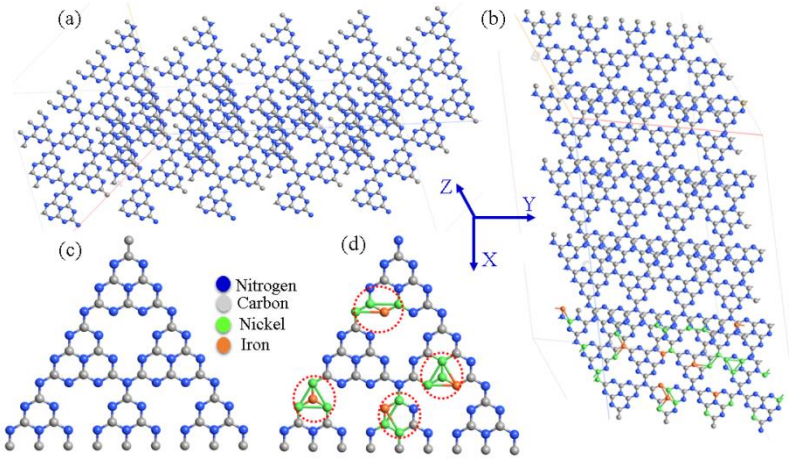

Figure 2.10: Surface atomic configuration of **(a)** g-C_3N_4 layer structure with a interplanner spacing of 12 Å, **(b)** composite of g-C_3N_4 and $FeNi_3$ where the $FeNi_3$ is stabilized on surface of the layer structure, monolayers of **(c)** g-C_3N_4 and **(d)** composite. Colour codes of the respective atoms are marked in the figure. Dotted red circle shows the presence of $FeNi_3$ on g-C_3N_4 surface.

2.7.2 Electronic structure of the system

The density of states (DOS) for the composite systems including graphitic sheet has been calculated to find the number of states of the sheets in pristine form and in composite form (shown in **Figure 2.11 (a)**). To understand the origin and control of sorption performance of active carbon and nitrogen sites in graphitic sheet and its composite with MNPs, the local densities of states (LDOSs) are performed (shown in **Figure 2.11 (b)**). Overlapping states are observed from the DOS and LDOS plots showing the active metallic behavior in the sheet and composite system. Presence of localized electrons on the Fe and Ni edges of g-C_3N_4@$FeNi_3$ composite system has contributed to the overlapping states at Fermi level within conduction band and improved conductivities with delocalized nature of the MNP active sites. Enhanced state intensity values are noticed in case of composite structures compared to its pristine sheet retaining active metallic behavior due to presence of MNPs in the composite. The active metallic edge sites of the MNPs are delocalized on the sheet, as a result the MNPs are loosely bound in the sheet surface.

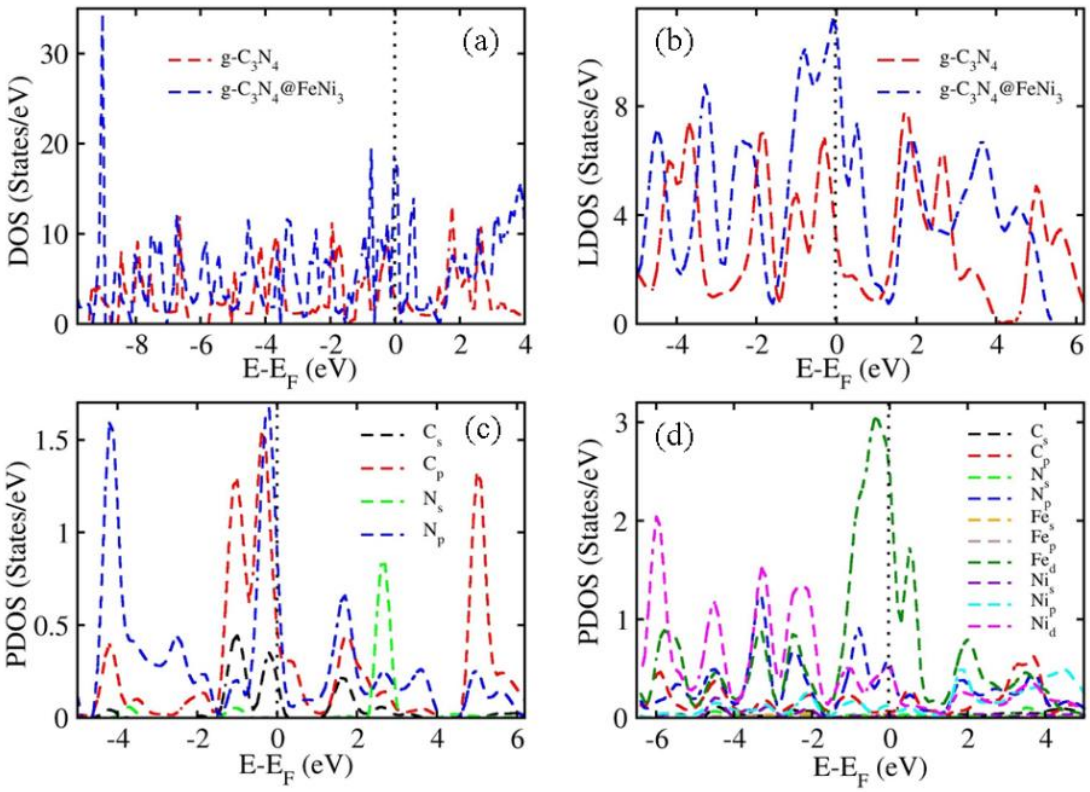

Figure 2.11: Electronic density of state pattern of both g-C_3N_4 and g-C_3N_4@$FeNi_3$ nanocomposite **(a)** DOS and **(b)** LDOS. Projected density of states (PDOS) for individual atomic orbitals shown in **(c)** for g-C_3N_4 and **(d)** g-C_3N_4@$FeNi_3$ nanocomposite. The Fermi level is denoted by black dotted lines at energy E_F = 0 eV.

To visualize the effect of orbital contribution on sorption activity, DOS have been projected to reciprocal space to obtain projected wave function values termed as projected density of states (PDOS). In our current study, carbon and nitrogen atoms have been considered in case of pristine graphitic sheet (shown in **Figure 2.11 (c)**) along with carbon, nitrogen, iron and nickel atoms (shown in **Figure 2.11 (d)**) to show the PDOS. This PDOS pattern reflects the orbital splitting and delocalized activity of the MNPs to form cluster like structures improving the sorption capability of the host sheet. The pattern indicates the orbital reflections of C_s, C_p, N_s, N_p, Fe_s, Fe_p, Fe_d, Ni_s, Ni_p and Ni_d which are necessary atomic orbitals to act upon for efficient sorption materials.

2.8 Conclusions

In this chapter, we have developed a novel and smart surface engineered sorbent material to realize magnetic separation of oil from oil-water mixtures. The stearic acid-based surface functionalized porous graphitic flakes exhibit not only wettability transition from hydrophilicity to hydrophobicity, but also selective oleophilicity in oil removal from water body. 2D graphitic flatland with precise surface area and high proportion of mesopore achieves high adsorption efficiency of crude oil. As a result, the sheet thickness enhanced upto 9 folds compared to the pristine one. The developed system efficiently recovers crude oil from water surface under an external magnet with a quick response resulting 4.5 times mass enhancement of the oil adsorbed nanocomposite, which is verified by pseudo second order adsorption kinetics. The adsorption study is in good agreement with the Freundlich isotherm indicating the efficient multilayer adsorption by the nanocomposite system. Apart from the crude oil, the composite system selectively adsorbs a wide range of oils. Thus, we conclude that the prepared g-C_3N_4@$FeNi_3$ nanocomposite will act as promising adsorbent material for efficient oil recovery and hence provide feasible solution towards the upcoming oil consumption.

References

[1]Lee, C., Q, Li., Kalb, W., Liu, X. Z., Berger, H., Carpick, R. W., and Hone, J. Frictional characteristics of atomically thin sheets. *Science,* 328:76-80, 2010.

[2]Jernelov, A. How to defend against future oil spills. *Nature,* 466:182-183, 2010.

[3]Keller, A. A., and Broje, V. Improved Mechanical Oil Spill Recovery Using an Optimized Geometry for the Skimmer Surface. *Environmental Science & Technology*, 40 (24):7914-7918, 2006.

[4]Choi, H. M., and Cloud, R. M. Natural sorbents in oil spill cleanup. *Environmental Science & Technology*, 26 (4):772-776, 1992.

[5]Adebajo, M. O., Frost, R. L., Kloprogge, J. T., Carmody, O., and Kokot, S. Porous Materials for Oil Spill Cleanup: A Review of Synthesis and Absorbing Properties. *Journal of Porous Materials,* 10 (3):159-170, 2003.

[6] Bayat, A., Aghamiri, S. F., Moheb, A., and Vakili-Nezhaad, G. R. Oil Spill Cleanup from Sea Water by Sorbent Materials. *Chemical Engineering & Technology*, 28 (12):1525-1528, 2005.

[7] Kujawinski, E. B., Soule, M. C. K., Valentine, D. L., Boysen, A. K., Longnecker, K., and Redmond, M. C. Fate of Dispersants Associated with the Deepwater Horizon Oil Spill. *Environmental Science & Technology,* 45(4):1298-1306, 2011.

[8] Aziz, H. A., Zahed, M. A., Isa, M. H., Mohajeri, L., and Mohajeri, S. A statistical experiment design approach for optimizing biodegradation of weathered crude oil in coastal sediments. *Bioresource Technology,* 101(24):9455-9460, 2010.

[9] Buist, I., McCourt, J., Potter, S., Ross, S., and Trudel, K. In situ burning. *Pure and Applied Chemistry,* 71:43-65, 1999.

[10] Kujawinski, E. B., Soule, M. C. K., Valentine, D. L., Boysen, A. K., Longnecker, K., and Redmond, M. C. Fate of dispersants associated with the Deepwater Horizon oil spill. *Environmental Science & Technology,* 45:1298-1306, 2011.

[11] Vidyasagar, A., Handore, K., and Sureshan, K. M. Soft optical devices from self-healing gels formed by oil and sugar-based organogelators. *Angewandte Chemie International Edition,* 50:8021-8024, 2011.

[12] Broje, V., and Keller, A. A. High thermal responsiveness of a reduced graphene oxide field-effect transistor. *Environmental Science & Technology*, 40:7914-7918, 2006.

[13] Tian, D. L., Zhang, X. F., Wang, X., Zhai, J., and Jiang, L. Thermally limited current carrying ability of graphene nanoribbons. *Physical Chemistry Chemical Physics*, 13(32):14606-14610, 2011.

[14] Sun, H., Xu, Z., and Gao, C. Multifunctional, Ultra-Flyweight, Synergistically Assembled Carbon Aerogels. *Advanced Materials*, 25:2554-2560, 2013.

[15] Si, Y., Yu, J., Tang, X., Ge, J., and Ding, B. Ultralight nanofibre-assembled cellular aerogels with superelasticity and multifunctionality. *Nature Communications*, 5:5802-5811, 2014.

[16] Li, K., Ju1, J., Xue, Z., Ma, J., Feng, L., Gao, S., and Jiang, L. Structured cone arrays for continuous and effective collection of micron-sized oil droplets from water. *Nature Communications,* 4:2276-2283, 2013.

[17] Naguib, M., and Gogotsi, Y. Synthesis of Two-Dimensional Materials by Selective Extraction. *Accounts of Chemical Research,* 48:128-135, 2015.

[18] Ge, B., Han, L., Liang, X., Li, F., Pu, X., Zhu, X., Zhang, Z., Shao, X., Jin, C., and Li, W. Fabrication of superhydrophobic Cu-BiOBr surface for oil/water separation and water soluble pollutants degradation. *Applied Surface Science,* 462:583-589, 2018.

[19] Liu, H., and Kang, Y. Superhydrophobic and superoleophilic modified EPDM foam rubber fabricated by a facile approach for oil/water separation. *Applied Surface Science,* 451:223-231, 2018.

[20] Giannozzi, P., Baroni, S., Bonini, N., Calandra, M., Car, R., Cavazzoni, C., Ceresoli, D., Chiarotti, G. L., Cococcioni, M., Dabo, I., Corso, A. D., Fabris, S., Fratesi, G., Gironcoli, S. D., Gebauer, R., Gerstmann, U., Gougoussis, C., Kokalj, A., Lazzeri, M., Martin-Samos, L., Marzari, N., Mauri, F., Mazzarello, R., Paolini, S., Pasquarello, A., Paulatto, L., Sbraccia, C., Scandolo, S., Sclauzero, G., Seitsonen, A. P., Smogunov, A., Umari, P., and Wentzcovitch, R. M. QUANTUM ESPRESSO: a modular and open-source software project for quantum simulations of materials. *Journal of Physics: Condensed Matter,* 21(39):395502-395522, 2009.

[21] Perdew, J. P., Ernzerhof, M., and Burke, K. Rationale for mixing exact exchange with density functional approximations. *The Journal of Chemical Physics,* 105 (22):9982-9987, 1996.

[22] Monkhorst, H. J., and Pack, J. D. Special points for Brillouin-zone integrations. *Physical Review B,* 13:5188-5192, 1976.